THE JOURNAL OF BIOLOGICAL CHEMISTRY VOL. 284, NO. 18, pp. 12041–12048, May 1, 2009


# Generation of Cubic Membranes by Controlled Homotypic Interaction of Membrane Proteins in the Endoplasmic Reticulum*[S]

Received for publication, January 12, 2009, and in revised form, February 25, 2009 Published, JBC Papers in Press, March 3, 2009, DOI 10.1074/jbc.M900220200

**Daniel Lingwood**[‡1], **Sebastian Schuck**[‡§], **Charles Ferguson**[‡¶], **Mathias J. Gerl**[‡], **and Kai Simons**[‡2]

*From the* [‡]*Max Planck Institute for Molecular Cell Biology and Genetics, 01307 Dresden, Germany, the* [§]*Department of Biochemistry and Biophysics, University of California at San Francisco, San Francisco, California 94158, and the* [¶]*Institute for Molecular Bioscience, University of Queensland, Brisbane, Queensland 4072, Australia*

**Cell membranes predominantly consist of lamellar lipid bilayers. When studied *in vitro*, however, many membrane lipids can exhibit non-lamellar morphologies, often with cubic symmetries. An open issue is how lipid polymorphisms influence organelle and cell shape. Here, we used controlled dimerization of artificial membrane proteins in mammalian tissue culture cells to induce an expansion of the endoplasmic reticulum (ER) with cubic symmetry. Although this observation emphasizes ER architectural plasticity, we found that the changed ER membrane became sequestered into large autophagic vacuoles, positive for the autophagy protein LC3. Autophagy may be targeting irregular membrane shapes and/or aggregated protein. We suggest that membrane morphology can be controlled in cells.**

The observation that simple mixtures of amphiphilic (polar) lipids and water yield a rich flora of phase structures has opened a long-standing debate as to whether such membrane polymorphisms are relevant for living organisms (1–7). Lipid bilayers with planar geometry, termed lamellar symmetry, dominate the membrane structure of cells. However, this architecture comprises only a fraction of the structures seen with *in vitro* lipid-water systems (7–11). The propensity to form lamellar bilayers (a property exclusive to cylindrically shaped lipids) is flanked by a continuum of lipid structures that occur in a number of exotic and probably non-physiological *non-bilayer* configurations (3, 12). However, certain lipids, particularly those with smaller head groups and more bulky hydrocarbon chains, can adopt *bilayered* non-lamellar phases called cubic phases. Here the bilayer is curved everywhere in the form of saddle shapes corresponding to an energetically favorable minimal surface of zero mean curvature (1, 7). Because a substantial number of the lipids present in biological membranes, when studied as individual pure lipids, form cubic phases (13), cubic membranes have received particular interest in cell biology.

Since the application of electron microscopy (EM)[3] to the study of cell ultrastructure, unusual membrane morphologies have been reported for virtually every organelle (14, 15). However, interpretation of three-dimensional structures from two-dimensional electron micrographs is not easy (16). In seminal work, Landh (17) developed the method of direct template correlative matching, a technique that unequivocally assesses the presence of cubic membranes in biological specimens (16). Cubic phases adopt mathematically well defined three-dimensional configurations whose two-dimensional analogs have been derived (4, 17). In direct template correlative matching, electron micrographs are matched to these analogs. Cubic cell membrane geometries and *in vitro* cubic phases of purified lipid mixtures do differ in their lattice parameters; however, such deviations are thought to relate to differences in water activity and lipid to protein ratios (10, 14, 18). Direct template correlative matching has revealed thousands of examples of cellular cubic membranes in a broad survey of electron micrographs ranging from protozoa to human cells (14, 17) and, more recently, in the mitochondria of amoeba (19) and in subcellular membrane compartments associated with severe acute respiratory syndrome virus (20). Analysis of cellular cubic membranes has also been furthered by the development of EM tomography that confirmed the presence of cubic bilayers in the mitochondrial membranes of amoeba (21, 22).

Although it is now clear that cubic membranes can exist in living cells, the generation of such architecture would appear tightly regulated, as evidenced by the dominance of lamellar bilayers in biology. In this light, we examined the capability and implications of generating cubic membranes in the endoplasmic reticulum (ER) of mammalian tissue culture cells. The ER is a spatially interconnected complex consisting of two domains, the nuclear envelope and the peripheral ER (23–26). The nuclear envelope surrounds the nucleus and is composed of two continuous sheets of membranes, an inner and outer nuclear membrane connected to each other at nuclear pores. The peripheral ER constitutes a network of branching trijunctional

* This work was supported by a European Union FP6 PRISM grant and Grant SP1175 from the Deutsche Forschungsgemeinschaft (to K. S.).
[S] The on-line version of this article (available at http://www.jbc.org) contains supplemental Figs. S1–S7.
[1] Recipient of an international Natural Science and Engineering Research Council post-graduate scholarship.
[2] To whom correspondence should be addressed: Pfotenhauerstrasse 108, 01307 Dresden, Germany. Fax: 49-351-210-1209; E-mail: simons@mpi-cbg.de.

[3] The abbreviations used are: EM, electron microscopy; ER, endoplasmic reticulum; OSER, organized smooth endoplasmic reticulum; LAT, linker of activated T-cells; VIP17/MAL, vesicular integral membrane protein 17/myelin and lymphocyte protein; IDER, inducible dimer; IMER, inducible multimer; $F_v$, homodimerization tag; AP20187, bifunctional membrane-permeable chemical dimerizer; EEA1, early endosome antigen 1; LAMP2, lysosomal-associated membrane protein 2; ER-phagy, an endoplasmic reticulum-specific autophagic process; mRFP, monomeric red fluorescent protein; GFP, green fluorescent protein; PBS, phosphate-buffered saline.

tubules that are continuous with membrane sheet regions that occur in closer proximity to the nucleus. Recently it has been suggested that the classical morphological definition of rough ER (ribosome-studded) and smooth ER (ribosome-free) may correspond to sheet-like and tubular ER domains, respectively (27). The ER has a strong potential for cubic architectures, as demonstrated by the fact that the majority of cubic cell membranes in the EM record come from ER-derived structures (14, 17). Furthermore, ER cubic symmetries are an inducible class of organized smooth ER (OSER), a definition collectively referring to ordered smooth ER membranes (=stacked cisternae on the outer nuclear membrane, also called Karmelle (28–30), packed sinusoidal ER (31), concentric membrane whorls (30, 32–34), and arrays of crystalloid ER (35–37)). Specifically, weak homotypic interactions between membrane proteins produce both a whorled and a sinusoidal OSER phenotype (38), the latter exhibiting a cubic symmetry (16, 39).

We were able to produce OSER with cubic membrane morphology via induction of homo-dimerization of artificial membrane proteins. Interestingly, the resultant cubic membrane architecture was removed from the ER system by incorporation into large autophagic vacuoles. To assess whether these cubic symmetries were favored in the absence of cellular energy, we depleted ATP. To our surprise, the cells responded by forming large domains of tubulated membrane, suggesting that a cubic symmetry was not the preferred conformation of the system. Our results suggest that whereas the endoplasmic reticulum is capable of adopting cubic symmetries, both the inherent properties of the ER system and active cellular mechanisms, such as autophagy, can tightly control their appearance.

## EXPERIMENTAL PROCEDURES

*Reagents and Antibodies*—The bifunctional dimerizer AP20187 along with the plasmid encoding its $F_v$ target domain ($pC_4$-$F_v$1E) was obtained from Ariad (Cambridge, MA). The American Type Culture Collection supplied the HeLa cell line. Dulbecco's modified Eagle's medium and Opti-MEM were from Invitrogen. IgG-Sepharose was purchased from Amersham Biosciences. Octyl-β-D-glucoside was from Glycon Biochemicals (Luckenwalde, Germany). Ultrapure sucrose was obtained from United States Biochemical Co. (Cleveland, OH). All protease inhibitors and other general reagents were purchased from Sigma.

Monoclonal antibodies against EEA1 and calnexin were from BD Transduction Laboratories. Giantin monoclonal antibody (40) was a gift from Hans-Peter Hauri (University of Basel, Basel, Switzerland), Monoclonal antibodies against LAMP2 and lysobisphosphatidic acid were provided by Lawrence Rajendran (MPI-CBG, Dresden, Germany) and Jean Gruenberg (University of Geneva, Switzerland), respectively. Monoclonal LC3 antibody (M152-3) was obtained from Medical and Biological Laboratories (Woburn, MA), and polyclonal anti-protein disulfide isomerase was purchased from Stressgen (Ann Arbor, MI). Alexa-488 conjugated secondary antibodies were purchased from Invitrogen.

*DNA Constructs*—GFP-cytochrome $b_5$ and Sec61γ-GFP (38) were gifts from Nica Borgese (University of Milan, Milan, Italy). GFP-LC3 was a gift from Stefan Jentsch (Max Planck Institute for Biochemistry, Martinsried, Germany). Inducible dimer constructs (generically termed IDER) were originally based on pSS-LAT-GFP (Ref. 41; backbone = pEGFP N1 (Clontech); SS = rabbit lyzophorin hydrolase signal sequence; LAT = transmembrane domain of the linker of activated T-cells). An Age1-mRFP-BsrG1 fragment from pmRFP (42) was inserted into AgeI/BsrG1-digested pSS-LAT-GFP generating pSS-LAT-mRFP. The PCR product BsrG1-$myc_3$-XbaI was inserted into the BsrGI/XbaI site of pSS-LAT-mRFP, which yielded pSS-LAT-RFP-$myc_3$. XbaI-$F_v$-SpeI was digested from $pC_4$-$F_v$1E and inserted into the XbaI site of pSS-LAT-mRFP-$myc_3$, generating pSS-LAT-mRFP-$myc_3$-$F_v$ (=LAT-IDER). For a tetraspanning transmembrane domain, VIP17/MAL from pBAT-VIP17 (43) was amplified with NheI/Age I overhangs and inserted into the NheI/Age I site of LAT-IDER, yielding VIP17-mRFP-$myc_3$-$F_v$ (=VIP-IDER). A recombinant adenovirus encoding LAT-IDER was generated as described (44).

*Generation of Recombinant Inducible Dimer and Multimer*—A PCR-generated NotI-Xho-mRFP-myc3-$F_v$-SalI fragment was fused to a C-terminal tandem affinity purification tag by insertion into the NotI/XhoI site of the linker-PreScission-TAP containing pFastBac vector (pFBLPT; linker = SSGPSGS; followed by the PreScission protease cleavage site LEVLFQ↓GP; pFB expression under the control of the polyhedrin promoter (Invitrogen)) (45). IDER was created via insertion of PCR-amplified NcoI-VIP17-XhoI fragments into the NcoI/XhoI-digested LPTpFB. Inducible multimer (termed IMER, contains three $F_v$ domains) was created by sequential insertion of XbaI-$F_v$-SpeI fragments into XbaI-digested IDER-LPTpFB. The recombinant baculovirus was generated according to the manufacturer's instructions (Invitrogen). VIP17-IDER/IMER were expressed and purified according to Kalvodova *et al.* (45).

*Velocity Gradient Centrifugation*—To evaluate the principle of induction of homo-dimerization/homo-oligomerization by the dimerizer AP20187, 25 μg of recombinant VIP17-IDER/IMER were incubated with or without 50 nM AP20187 in 100 μl of TNE gradient buffer (10 mM Tris, 200 mM NaCl, 1 mM EDTA, 60 mM octyl-β-D-glucoside, pH 7.4) with protease inhibitors (25 μg/ml chymostatin, 25 μg/ml leupeptin, 25 μg/ml antipain, 25 μg/ml pepstatin) for 1 h at 4 °C. The protein solution was then loaded on a 2.1-ml 5–20% continuous sucrose gradient ("ultrapure" sucrose (United State Biochemical) in TNE gradient buffer plus protease inhibitors) in Ultraclear centrifuge tubes (11 × 34 mm, Beckman) and centrifuged in a TLS-55 rotor (Beckman) at 200 000 × *g* for 8 h. The gradient was separated into 26 fractions and immunoblotted with an anti-mRFP mouse monoclonal antibody (Antibody Facility, MPI-CBG).

*Immunoblotting*—Separation of proteins by SDS-PAGE was on 12% Tris-glycine gels. Immunoblotting was performed after transfer to methanol-activated polyvinylidene difluoride membranes. Blots were developed with ECL detection reagents, and the chemiluminescence signals were detected using Hyperfilm ECL (Amersham Biosciences).

*Cell Culture and Transfection/Infection*—HeLa cells were grown in Dulbecco's modified Eagle's medium supplemented with 10% fetal calf serum, glutamate, penicillin, and streptomycin. Transient transfections were performed in 24-well format (Nunc, Roskilde, Denmark) using Lipofectamine 2000 (Invitrogen) according to the manufacturer's instructions. The recom-

binant adenovirus encoding LAT-IDER was used to increase the fraction of expressing cells compared with Lipofectamine-mediated transient transfection. For infection, 3 μl of virus were added to 500 μl of Opti-MEM in 3.5-cm plastic dishes (Nunc) and incubated with 80% confluent HeLa cells for 2 h. Opti-MEM was then replaced with Dulbecco's modified Eagle's medium. For OSER production, cells were transfected or infected in the presence of 50 nM AP20187.

*Immunofluorescence Microscopy*—Cells were fixed with formaldehyde, permeabilized with 0.1% (w/v) Triton-X100 (for LC3 immunofluorescence, cells were fixed and permeabilized with methanol at −20 °C), and incubated with primary and Alexa-488-conjugated secondary antibodies. Monodansylcadaverine staining was according to Biederbick *et al.* (46). Microscopy was performed at room temperature with confocal microscopy systems (models LSM UV and LSM 405/594 from Carl Zeiss, Jena, Germany); Alexa-488, mRFP, and monodansylcadaverine were excited at 488, 594, and 350 nm, respectively. A 63 × 1.4 NA oil objective was employed throughout.

*Electron Microscopy*—Cells were first washed quickly in PBS. Immediately after rinsing, dishes were flooded with a 2.5% solution of glutaraldehyde in PBS for 60 min at room temperature. Thereafter, the fixative was rinsed away with PBS (3 × 5 min), and an aqueous solution (1%) of osmium tetroxide was added and left for 60 min. The osmium solution was washed out with water (4 × 5 min). Cells were further incubated at 4 °C in an aqueous solution containing 4% uranyl acetate for 60 min. Cells were dehydrated by washing with 4% uranyl acetate in 70% ethanol for 10 min followed by three 3-min washes with pure ethanol. They were then embedded in Epon LX112. The final resin was polymerized in an oven at 60 °C overnight. Ultra-thin sections (60–90 nm) for ultrastructural examination were cut on a Leica Ultracut UCT microtome and mounted on Formvar-coated copper grids. Grids were post-stained with 5% uranyl acetate in 50% methanol for 3 min and aqueous lead citrate for 90 s. Sections were viewed on a FEI Tecnai 12 transmission electron microscope (FEI, Eindhoven, The Netherlands) at 100 kV.

*Energy Depletion Experiments*—For depletion of cellular ATP, HeLa cells were incubated in PBS containing 1 mM $CaCl_2$ and 1 mM $MgCl_2$ ($PBS^{2+}$) supplemented with 10 mM 2-deoxy-D-glucose and 10 mM $NaN_3$ for 2 h at 37 °C (47). Samples were then immediately fixed and processed for electron microscopy as described above.

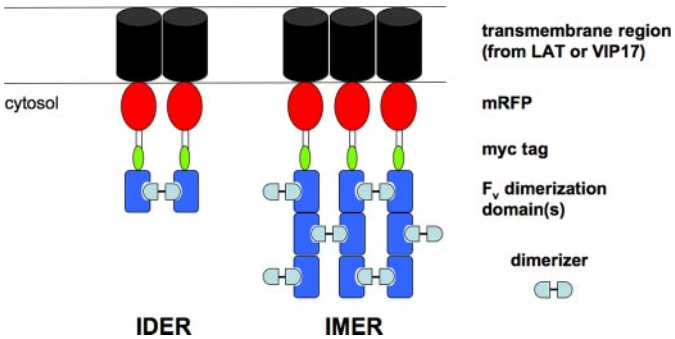


FIGURE 1. **IDER and IMER constructs.** IDER and IMER are chimeric proteins consisting of a transmembrane region (LAT (single spanning) or VIP17 (tetraspanning)), fused to a cytosolic mRFP-myc-$F_v$, where mRFP = monomeric red fluorescent protein, myc = three myc tags, and $F_v$ = a homodimerization domain that binds to the membrane-permeable bifunctional dimerizer AP20187. IDER contains one $F_v$ domain; IMER contains three. Both constructs are expected to be monomeric in the absence of dimerizer, to form dimers and oligomers, respectively, in its presence.

## RESULTS

*Dimerization Domain-mediated Self-assembly Tested in Vitro*—Previous studies have shown that the architecture of the ER can be altered by the expression of ER membrane proteins with a propensity to oligomerize. To be able to assess the contribution of protein oligomerization to this phenomenon, we sought to construct artificial membrane proteins whose oligomeric state can be tightly regulated. For this purpose we fused the transmembrane regions of LAT or VIP17 to mRFP, a myc tag, and one or three copies of the $F_v$ dimerization domain. The resulting constructs were called LAT-IDER/VIP17-IDER and LAT-IMER/VIP17-IMER, where IDER and IMER stand for "inducible dimer" and "inducible multimer," respectively (Fig. 1). The presence of the $F_v$ domains allows the application of homodimerization technology developed by Ariad, which is based on the structure of FKBP12 (FK506 binding protein 12). FKBP12 is a ubiquitous peptidyl-prolyl cis-trans isomerase, which is the target of the immunosuppressive drug FK506 (48). Artificial specificity is achieved by introduction of a steric clash ("bump") into a bifunctional chemical dimerizer (termed AP20187) that binds with high affinity to a correspondingly sterically modified ("holed") FKBP12 variant, termed $F_v$, abolishing binding to endogenous FKBP. This principle of controlled dimerization by $F_v$-tagged membrane proteins was first tested *in vitro* with recombinant VIP17-IDER and VIP17-IMER.

Recombinant VIP17-IDER and VIP17-IMER were purified, and their capacity to dimerize or oligomerize after the addition of the dimerizer was evaluated by velocity gradient sedimentation through a continuous sucrose gradient. Exposure of recombinant VIP17-IDER/IMER to 50 nM AP20187 before centrifugation shifted their sedimentation distributions toward a higher molecular weight (Fig. 2). This shift was more pronounced for the VIP17-IMER, indicating a correlation between the number of $F_v$ domains and the degree of self-association.

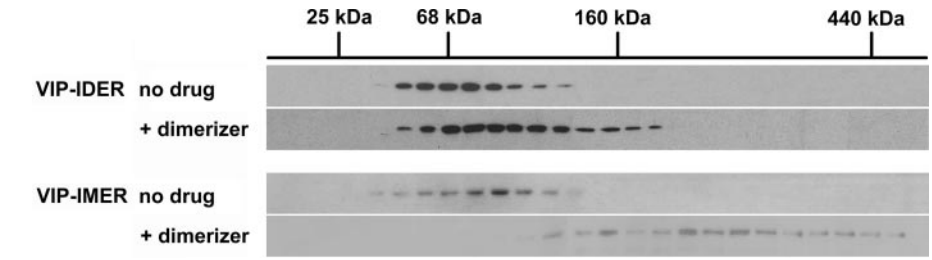


FIGURE 2. **IDER and IMER oligomerize *in vitro*.** Controlled homo-oligomerization was assessed by velocity gradient centrifugation of purified recombinant-inducible dimer (VIP17-IDER, one $F_v$ domain) and multimer (VIP17-IMER, three $F_v$ domains). The gradient was fractionated and immunoblotted with an anti-mRFP mouse monoclonal antibody. Compared with controls (no drug), AP20187-treated protein (+dimerizer) displayed higher order assemblages for both $F_v$ arrangements, although most strikingly for IMER, indicating that the number of $F_v$ domains correlates with the degree of self-association *in vitro*.

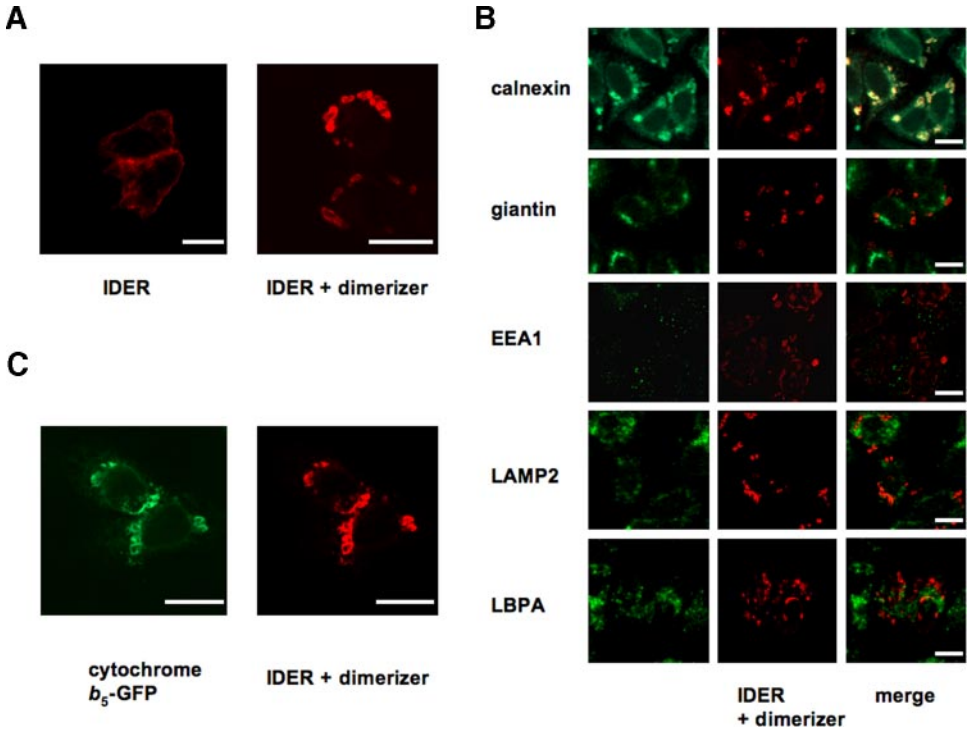


FIGURE 3. **IDER dimerization *in vivo*.** When expressed in HeLa cells, LAT-IDER and VIP17-IDER traveled to the plasma membrane unless cells were incubated with the dimerizer, in which case IDER was found in large micron-scale membrane structures (*A*). These structures were positive for cotransfected ER-residing cytochrome $b_5$-GFP (*B*) and immuno-positive for the ER marker calnexin but not for markers of the Golgi (giantin), early endosomes (*EEA1*), lysosomes (*LAMP2*), or multivesicular bodies (*LBPA*), indicating that they derive from the ER (*C*). *Scale bar* = 10 $\mu$m.

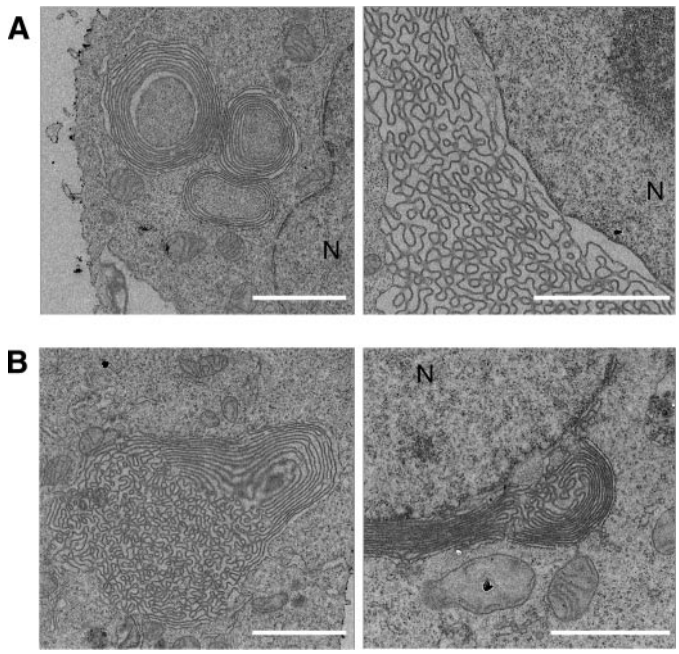


FIGURE 4. **Ultrastructure of IDER-induced OSER.** Cells were infected with an adenovirus encoding LAT-IDER, grown in presence of dimerizer fixed in glutaraldehyde, and processed for electron microscopy. The ER was seen as whorled and sinusoidal ribosome-free membranes (*A*), which sometimes occurred as part of the same structure (*B*), indicating that these membrane architectures may represent different stages of the same membrane re-organization. *N* = nucleus; *scale bar* = 5 $\mu$m.

*$F_v$-mediated Dimerization Generates OSER in Vivo*—When introduced into HeLa cells, LAT-IDER and VIP17-IDER trafficked to the plasma membrane, indicating that these constructs were properly folded (Fig. 3*A*). However, if transfection or infection of HeLa cells with IDER-encoding vectors was carried out in the presence of the membrane-permeable dimerizer AP20187, both LAT-IDER and VIP17-IDER became concentrated within intracellular micron-sized structures (Fig. 3*B*). These structures could also be induced by adding the dimerizer to cells already producing LAT-IDER or VIP17-IDER, in this case appearing after 3–4 h of exposure to 50 nM AP20187 (not shown). For both single-spanning and tetraspanning IDER, the structures stained positive for the ER marker calnexin (Fig. 3*C*), which no longer showed the reticular distribution characteristic of the ER in unperturbed cells (supplemental Fig. S1). Moreover, this ER morphology was not seen in the presence of the dimerizing drug alone (supplemental Fig. S2). IDER-positive structures also colocalized with cytochrome $b_5$-GFP, another protein that labels the ER (49) (Fig. 3*B*). Indeed, the ER-residing protein disulfide isomerase and Sec61$\gamma$-GFP were also enriched (supplemental Fig. S3). Immunofluorescence indicated that these structures did not contain membrane markers of the Golgi (giantin), early endosomes (*EEA1*), lysosomes (*LAMP-2*), or multivesicular bodies (*LBPA*) (Fig. 3*C*). Similar results were obtained for LAT-IMER and VIP-IMER variants (not shown).

These data show that the presence of the dimerizing drug causes ER retention of the IDER constructs. They also suggest that $F_v$-mediated dimerization of LAT/VIP17-IDER produced a remodeling of ER membranes reminiscent of the formation of organized smooth ER (OSER), previously observed after expression of GFP fusion proteins with a tendency to dimerize (38). For OSER produced by homotypic interactions between membrane proteins, two distinct but coincident architectural ER subclasses have been described; that is, a whorled and a sinusoidal membrane organization (38), where the sinusoidal pattern conforms to a cubic symmetry (16, 39). EM revealed that our IDER-induced ER phenotype corresponded to both OSER subtypes (Fig. 4*A*). Interestingly, sinusoidal OSER membranes could sometimes be seen in an apparent conversion to whorled OSER architecture (Fig. 4*B*), indicating that these OSER subtypes may represent different developmental stages of the same membrane re-organization. Furthermore, the sinusoidal membrane morphology could be matched to a two-

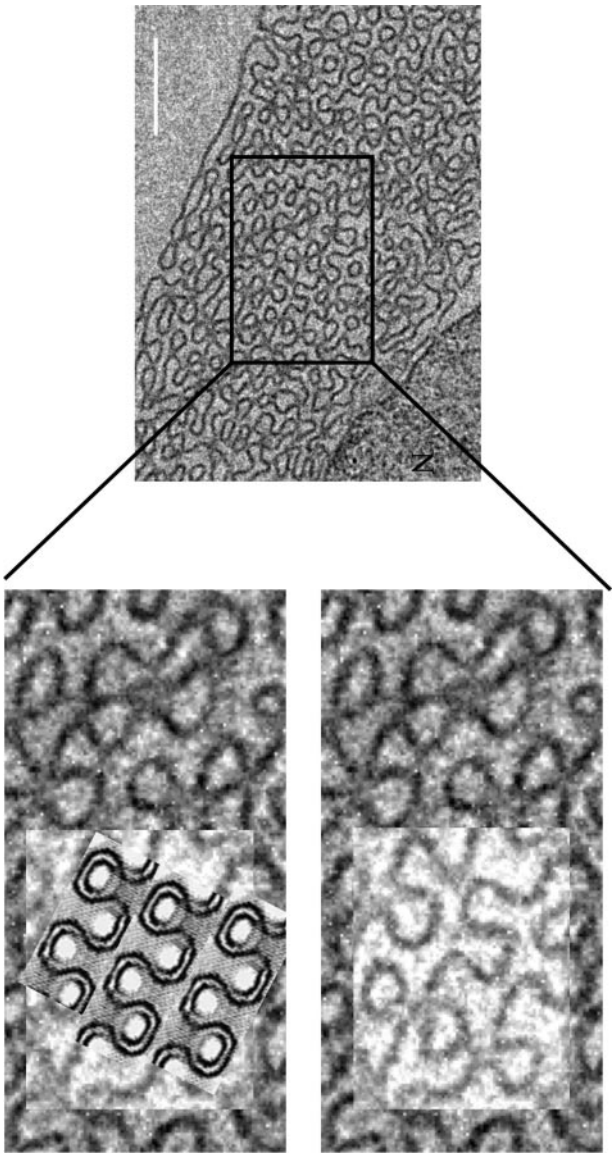


FIGURE 5. **Cubic symmetry of sinusoidal OSER.** Template matching showed that sinusoidal OSER has cubic geometry, as it could be matched to a two-dimensional representation of a three-dimensional double diamond cubic symmetry. This two-dimensional analog of cubic symmetry was obtained from a library of projections generated by Mieckowski and Landh (unpublished information). The two-dimensional analog was manually superimposed on the electron micrograph (Landh (14, 17)). *Scale bar* = 1.5 $\mu$m.

dimensional template representing double diamond cubic symmetry (14, 17) (Fig. 5).

*OSER Is Incorporated into Autophagic Vacuoles*—EM revealed that proliferations of sinusoidal/cubic OSER were often situated either proximal to or within large vacuoles (Fig. 6*A*). Whorled OSER could also be targeted for vacuolar engulfment (Fig. 6*B*). These vacuoles stained with the acidotropic dye monodansylcadaverine (Fig. 7*A*), showing that the vacuoles have a low pH and suggesting that the OSER had become subject to autophagic sequestration into a degradative compartment. Immunofluorescence microscopy showed that OSER membrane stained positive for the autophagy protein LC3 (Fig. 7*B*). A similar localization to OSER membranes was observed for an exogenous GFP-LC3 construct (supplemental Fig. S4). In

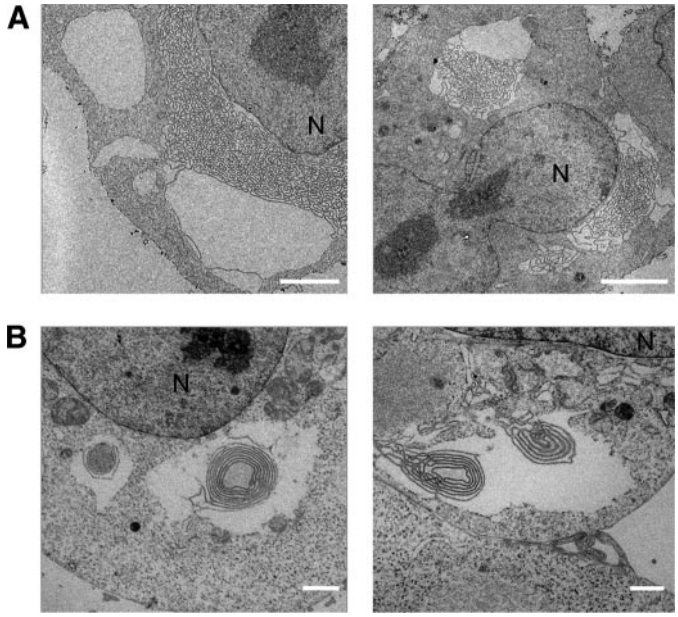


FIGURE 6. **Sequestration of sinusoidal and whorled OSER in large vacuoles.** Large proliferations of sinusoidal OSER membrane were typically situated directly proximal to or within large vacuoles (*A*); similarly whorled OSER could be vacuolarized (*B*), suggesting selective autophagy of these membranes. *N* = nucleus; *scale bar* = 5 $\mu$m in *A* and 1 $\mu$m in *C*.

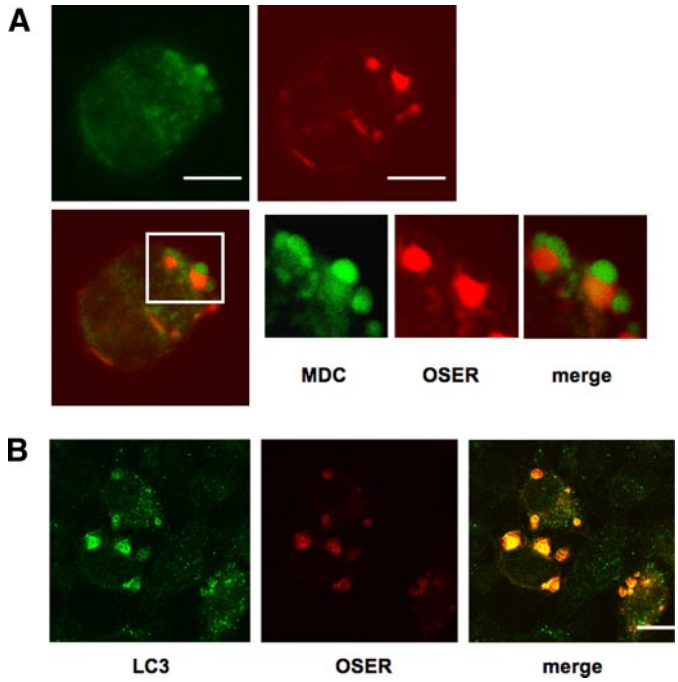


FIGURE 7. **Sequestration of OSER into acidic vacuoles and colocalization with the autophagic marker protein LC3.** IDER-induced OSER was often co-packaged with large vacuoles that stained positive for monodansylcadaverine (*MDC*), an *in vivo* marker of acidic degradative compartments (*A*). Whorled OSER was positive for LC3, indicating that artificial generation of OSER triggers an autophagic response (*B*). The sinusoidal membrane pattern of cubic OSER could not be optically resolved with confocal microscopy. *Scale bar* = 10 $\mu$m.

cells not expressing IDER, the dimerizing drug did not change the native pattern of LC3 staining (supplemental Fig. S5). Both endogenous LC3 and GFP-LC3 showed an even cytoplasmic distribution when IDER was expressed in the absence of the dimerizer (data not shown). These observations suggest that $F_v$

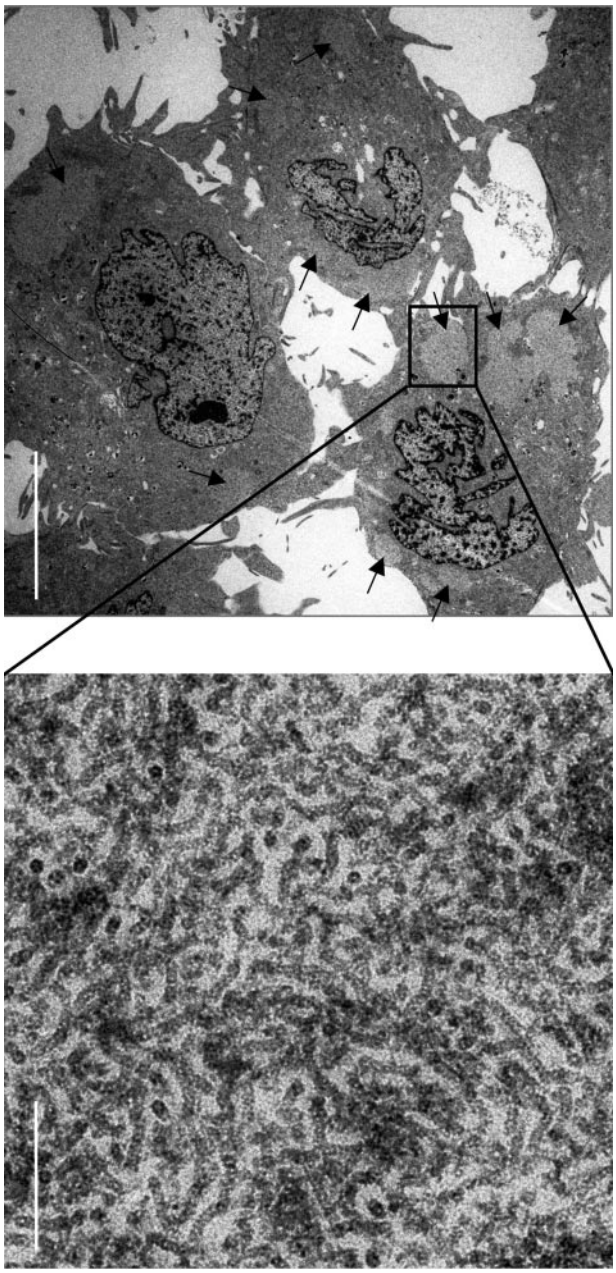

FIGURE 8. **ER membranes are poised for tubulation.** In the absence of cellular ATP large areas of tubulated membrane (*arrows*) began to appear after 2 h. *Scale bars* are 10 $\mu$m and 150 nm at low and high magnification, respectively.

dimerization between membrane proteins in the ER may be related to an autophagic response wherein the ensuing OSER whorls and sinusoids are removed from the ER.

*ER Membrane Tabulates after ATP Depletion*—Given that most biological lipids spontaneously form non-lamellar structures in lipid-water systems (13), we hypothesized that the cell may spend energy to maintain the ER as a lamellar reticulum. We, therefore, depleted cellular energy according to established pharmacological protocols (47) and assessed the ultrastructure of the ER by EM. After a 2-h energy block, cubic membranes did not appear; rather, we observed the emergence of new domains of tubulated membrane (Fig. 8).

## DISCUSSION

Homotypic interaction between membrane proteins through low affinity dimerization of a GFP tag was shown to induce whorled and sinusoidal OSER phenotypes in living cells (38). Direct template correlative matching later established that the sinusoidal ER architecture corresponded to a double diamond cubic symmetry (16). OSER induction by homotypic interaction, therefore, represents a valuable tool to study cubic membrane formation and its potential functions. To expand the controllability of this approach, we introduced an $F_v$ homodimerization tag fused to the cytosolic domain of transmembrane proteins to create inducible dimers. Expression of these constructs in the presence of the membrane-permeable dimerizer prevented their exit from the ER and converted this membrane system into OSER. EM confirmed both the whorled and sinusoidal ultrastructure of this phenotype. Furthermore, we could identify a double-diamond cubic symmetry in our sinusoidal OSER. Earlier EM studies have concluded that OSER structures connect to the rest of the ER (34, 35, 37, 38). Along these lines, we show that both the whorled and sinusoidal phenotypes can be associated with the same structure. This is consistent with the hypothesis that these forms of OSER represent different developmental stages of membrane re-organization (33, 36).

Attempts to understand the mechanism of OSER formation have largely concentrated on analyzing the whorled membrane phenotype. It was argued that binding interactions between cytoplasmic domains of ER resident proteins act to cross-link membranes into a compacted structure (33, 37, 50). However, this model was not supported by FRAP analyses showing that OSER-inducing proteins could readily diffuse in and out of OSER structures, indicating they were not tightly cross-linked to each other or to some type of scaffold (38). Nevertheless, the behavior of dimeric and monomeric GFP membrane constructs demonstrated the importance of weak homotypic interactions (presumably in *trans*) between the cytosolic domains of overexpressed membrane proteins in OSER induction (38). Consistent with this notion, our constructs employing cytosolic-based $F_v$ dimerization produced whorled OSER in which the cytoplasmic layer separating membrane stacks was of constant width (Fig. 4*A*). However, as with all reports in the OSER literature, the distinction between the role of membrane proliferation and membrane protein dimerization cannot be made; *i.e.* is dimerization itself sufficient to drive OSER formation, or is the phenomenon intrinsically linked to the expansion of the ER that accompanies the overexpression of ER membrane proteins?

Nevertheless, we offer a new hypothesis as to how OSER could adopt cubic symmetry in the form of double diamond sinusoids. *In vitro*, lipid polymorphism is a result of chemistry alone (1). In this respect, the departure from lamellar morphologies in cells may involve the activation of a lipid-based membrane-organizing principle. A substantial number of the lipids found in biological membranes have a propensity to form cubic bilayers *in vitro* (13). Indeed, cubic membranes represent periodic minimal surfaces (1, 7), *i.e.* the only alternative bilayer architecture with thermodynamically favorable zero net curva-

ture. However, biological membranes are mostly lamellar, implying that lipids are arranged both with each other and with proteins (*e.g.* through selective macromolecular assemblies, specific bilayer asymmetries etc) to make the lamellar state more favorable. Consequently, biological membranes are thought to have intrinsic lamellar instability (51), and it has been proposed that this stress field can be released in association with protein conformational changes (13, 52). We now suggest that widespread homo-dimerization between membrane proteins in the ER could unlock the non-lamellar potential residing within this organelle, allowing for dramatic micron-scale architectural reorganization requiring little or no cellular energy. This would be in agreement with the findings of Snapp *et al.* (38), where overexpression of weakly dimerizing membrane proteins induce cubic membrane symmetries in the ER. Moreover, we note that dimerization of IDER in the ER lumen (where there is no possibility of cytosolic transmembrane zippering) also produces OSER (supplemental Fig. S6). This suggests OSER membrane polymorphisms may arise from a capacity for architectural plasticity that resides within the membrane itself. Along these lines, we observed that OSER and OSER-associating membranes displayed high levels of cholesterol (supplemental Fig. S7), a non-lamellar-forming lipid (13). This was interesting as ER cholesterol concentration is normally kept low in accordance with the sterol-sensing function of this organelle (53). Indeed, a lipid storage function for OSER has been suggested (38); whether cholesterol sorting relates to preferences for certain membrane polymorphisms and/or autophagic processing (see below) remains to be investigated. In any event, it is generally accepted that ER subdomain formation occurs by self-organizing principles that allow for rapid transformation into alternative structures in response to altered conditions (39). Non-lamellar capability may be a factor in these processes.

Using EM, we observed that proliferations of OSER-derived cubic membrane were often proximal to or selectively engulfed within large vacuoles. The whorled OSER membrane was also targeted for vacuolization. At the level of fluorescence confocal microscopy, OSER was closely associated with the autophagy protein LC3 and often appeared inside vacuoles that stained with monodansylcadaverine. Unlike originally proposed (46), this dye does not stain autophagosomes, which have neutral pH but acidic degradative compartments, including autophagic vacuoles (54). We, therefore, suggest that $F_v$ dimerization-derived OSER was targeted by the autophagy machinery and is subsequently sent for degradation. Autophagy can mediate the elimination of stressed or damaged cytoplasmic organelles. For example, pexophagy and mitophagy are highly selective processes that degrade excess peroxisomes and mitochondria (55, 56). How selectivity during these processes is regulated is not clear. ER stress is a major stimulator of an autophagic response (termed ER-phagy) that may participate in the degradation of unfolded proteins and in the removal of damaged or superfluous ER membranes (57, 58). Recently, it was shown that an ER-specific autophagic process is used to counterbalance ER stress during the unfolded protein response in yeast (59). Along these lines, autophagy in our system may be related to the $F_v$-mediated protein aggregation responsible for OSER formation. Additionally, there is the possibility that ER-phagy is related to the morphology of the target. Indeed, the appearance of concentric membranous whorls and other architectural abnormalities such as deformed mitochondria have been reported in mice deficient for *Atg7* (an essential gene for autophagy), suggesting a role for autophagy in the maintenance of subcellular structural integrity (60).

Results from our OSER system would suggest that cubic membranes can be formed from protein dimerization in the ER but that there may be mechanisms in place that prevent exaggeration of the process. Given this potential for cubic membranes, we were interested in ER structure under conditions of low cellular energy. Surprisingly, the emergence of large areas of membrane tubulation was noted. It is possible that suppression of energy-dependent membrane fission events contributed to locking membrane traffic into tubular arrangements. The generation of tubules resulting from inhibition of membrane fission machinery has been reported, most notably in situations when protein kinase D activity is impaired (61). Moreover, emerging work on reticulons, a group of ER proteins that induce membrane network formation both in cells and in model membrane systems (26, 62), suggests that their capacity for tubule formation is inversely related to ATP availability, predicting increases in tubulation during ATP minima (63). Still, the molecular details underlying our tubulation phenotype are unclear; however, it suggests that cells do not expend ATP to prevent proliferation of cubic membrane architectures in the ER.

To summarize, we have shown that the ER membrane contains the potential for cubic symmetries in the form of sinusoidal OSER produced by $F_v$-mediated dimerization of membrane proteins. However, the OSER membranes were also removed from the ER system. The nature of this autophagic response is not clear; however, we assert that the inherent properties of the ER do not favor non-lamellar configurations. Rather, it appears that a preference for a tubular network is built into the ER. Although cubic symmetries do constitute a novel means of space-re-organization, our study suggests that both intrinsic properties of the ER system and active cellular mechanisms, such as autophagy, can control their appearance.

*Acknowledgments—We thank T. Landh (Novo Nordisk, Sweden), T. Rapoport (Harvard Medical School, Boston), L. Rajendran, U. Coskun, and the members of the Simons laboratory for helpful discussion. We also thank D. Vorkel (MPI-CBG) for technical assistance with EM imaging, and R. Lemaitre for aid during protein purification.*

## REFERENCES

1. Luzzati, V. (1968) in *Biological Membranes* (Chapman, D., ed) pp. 71–123, Academic Press, Inc., New York
2. Cullis, P. R., and de Kruijff, B. (1979) *Biochim. Biophys. Acta* **559,** 399–420
3. Mariani, P., Luzzati, V., and Delacroix, H. (1988) *J. Mol. Biol.* **204,** 165–189
4. Larsson, K. (1989) *J. Phys. Chem.* **93,** 7304–7314
5. Lindblom, G., and Rilfors, L. (1989) *Biochim. Biophys. Acta* **988,** 221–256
6. Bouligand, Y. (1991) in *Geometry in Condensed Matter Physics* (Sadoc, J. F., ed) pp. 193–231, World Scientific Press, London
7. Luzzati, V., Vargas, R., Mariani, P., Gulik, A., and Delacroix, H. (1993) *J. Mol. Biol.* **229,** 540–551
8. Marsh, D. (1990) *Handbook of Lipid Layers*, CRC Press, Boca Raton, FL

9. Seddon, J. (1990) *Biochim. Biophys. Acta* **1031,** 1–60
10. Bouligand, Y. (1990) *J. Phys. (Fr.) Coll.* **C7,** 35–52
11. Caffrey, M. (1993) *Lipidat*, CRC Press, Boca Raton, FL
12. Hui, S-W. (1987) *Comments Mol. Cell Biophys.* **4,** 233–248
13. Mouritsen, O. G. (2005) *Life - as a Matter of Fat: The Emerging Science of Lipodomics*, Springer-Verlag, Berlin
14. Landh, T. (1996) *Cubic Cell Membrane Structures*. Ph.D. thesis. Lund University, Lund, Sweden
15. Federovitch, C. M., Ron, D., and Hampton, R. Y. (2005) *Curr. Opin. Cell Biol.* **17,** 409–414
16. Almsherqi, Z. A., Kohlwein, S. D., and Deng, Y. (2006) *J. Cell Biol.* **173,** 839–844
17. Landh, T. (1995) *FEBS Lett.* **369,** 13–17
18. Brandenburg, K., Koch, M. H. J., and Seydel, U. (1992) *J. Struct. Biol.* **108,** 93–106
19. Deng, Y., and Mieczkowski, M. (1998) *Protoplasma* **203,** 16–25
20. Almsherqi, Z. A., McLachlan, C. S., Mossop, P., Knoops, K., and Deng, Y. (2005) *Redox Rep*. **10,** 167–171
21. Deng, Y., Marko, M., Buttle, K. F., Leith, A., Mieczkowski, M., and Mannella, C. A. (1999) *J. Struct. Biol.* **127,** 231–239
22. Deng, Y., Kohlwein, S. D., and Mannella, C. A. (2002) *Protoplasma* **219,** 160–167
23. Baumann, O., and Walz, B. (2001) *Int. Rev. Cytol.* **205,** 149–214
24. Du, Y., Ferro-Novick, S., and Novick, P. (2004) *J. Cell Sci.* **117,** 2871–2878
25. Voeltz, G. K., Rolls, M. M., and Rapoport, T. A. (2002) *EMBO Rep.* **3,** 944–950
26. Voeltz, G. K., Prinz, W. A., Shibata, Y., Rist, J. M., and Rapoport, T. A. (2006) *Cell* **124,** 573–586
27. Shibata, Y., Voeltz, G. K., and Rapoport, T. A. (2006) *Cell* **126,** 435–439
28. Smith, S., and Blobel, G. (1994) *Proc. Natl. Acad. Sci. U. S. A.* **91,** 10124–10128
29. Parrish, M. L., Sengstag, C., Rine, J. D., and Wright, R. L. (1995) *Mol. Biol. Cell* **6,** 1535–1547
30. Koning, A. J., Roberts, C. J., and Wright, R. L. (1996) *Mol. Biol. Cell* **7,** 769–789
31. Anderson, R. G., Orci, L., Brown, M. S., Garcia-Segura, L. M., and Goldstein, J. L. (1983) *J. Cell Sci.* **63,** 1–20
32. Feldman, D., Swarm, R. L., and Becker, J. (1981) *Cancer Res.* **41,** 2151–2162
33. Takei, K., Mignery, G. A., Mugnami, E., Sudhof, T. C., and De Camilli, P. (1994) *Neuron* **12,** 327–432
34. Gong, F. C., Giddings, T. H., Meehl, J. B., and Staehelin, L. A. (1996) *Proc. Natl. Acad. Sci. U. S. A*. **93,** 2219–2223
35. Chin, D. J., Luskey, K. L., Anderson, R. G., Faust, J. R., Goldstein, J. L., and Brown, M. S. (1982) *Proc. Natl. Acad. Sci. U. S. A.* **79,** 1185–1189
36. Pathak, R. K., Luskey, K. L., and Anderson, R. G. W. (1986) *J. Cell Biol.* **102,** 2158–2168
37. Yamamoto, A., Masaki, R., and Tashiro, Y. (1996) *J. Cell Sci.* **109,** 1727–1738
38. Snapp, E. L., Hegde, R. S., Francolini, M., Lombardo, F., Colombo, S., Pedrazzini, E., Borgese, N., and Lippincott-Schwartz, J. (2003) *J. Cell Biol.* **163,** 257–269
39. Borgese, N., Francolini, M., and Snapp, E. (2006) *Curr. Opin. Cell Biol.* **18,** 358–364
40. Linstedt, D., and Hauri, H. P. (1993) *Mol. Biol. Cell* **4,** 679–693
41. Meder, D., Moreno, M. J., Verkade, P., Vaz, W. L., and Simons, K. (2006) *Proc. Natl. Acad. Sci. U. S. A.* **103,** 329–334
42. Campbell, R. E., Tour, O., Palmer, A. E., Steinbach, P. A., Baird, G. S., Zacharias, D. A., and Tsien, R. Y. (2002) *Proc. Natl. Acad. Sci. U. S. A.* **99,** 7877–7882
43. Zacchetti, D., Peranen, J., Murata, M., Fiedler, K., and Simons, K. (1995) *FEBS Lett.* **375,** 465–469
44. He, T. C., Zhou, S., da Costa, L. T., Yu, J., Kinzler, K. W., and Vogelstein, B. (1998) *Proc. Natl. Acad. Sci. U. S. A.* **95,** 2509–2514
45. Kalvodova, L., Kahya, N., Schwille, P., Ehehalt, R., Verkade, P., Drechsel, D., and Simons, K. (2005) *J. Biol. Chem.* **280,** 36815–36823
46. Biederbick, A., Kern, H. F., and Elsässer, H. P. (1995) *Eur. J. Cell Biol.* **66,** 3–14
47. Zha, X., Pierini, L. M., Leopold, P. L., Skiba, P. J., Tabas, I., and Maxfield, F. R. (1998) **140,** 39–47
48. Clackson, T., Yang, W., Rozamus, L. W., Hatada, M., Amara, J. F., Rollins, C. T., Stevenson, L. F., Magari, S. R., Wood, S. A., Courage, N. L., Lu, X., Cerasoli, F., Jr., Gilman, M., and Holt, D. A. (1998) *Proc. Natl. Acad. Sci. U. S. A.* **95,** 10437–10442
49. Bulbarelli, A., Sprocati, T., Barberi, M., Pedrazzini, E., and Borgese, N. (2002) *J. Cell Sci.* **115,** 1689–1702
50. Fukuda, M., Yamamoto, A., and Mikoshiba, K. (2001) *J. Biol. Chem.* **276,** 41112–41119
51. Gruner, S. M. (1985) *Proc. Natl. Acad. Sci. U. S. A.* **82,** 3665–3669
52. Kinnunen, P. (1992) *Chem. Phys. Lipids* **63,** 251–258
53. Ikonen, E. (2008) *Nat. Rev. Mol. Cell Biol.* **9,** 125–138
54. Klionsky, D. J., *et al.* (2008) *Autophagy* **16,** 151–175
55. Dunn, W. A., Jr., Cregg, J. M., Kiel, J. A., van der Klei, I. J., Oku, M. Sakai, Y., Sibirny, A. A., Stasyk, O. V., and Veenhuis, M. (2005) *Autophagy* **1,** 75–83
56. Kundu, M., and Thompson, C. B. (2005) *Cell Death Differ.* **12,** 1484–1489
57. Bernales, S., Schuck, S., and Walter, P. (2007) *Autophagy* **3,** 285–287
58. Yorimitsu, T., and Klionsky, D. J. (2007) *Trends Cell Biol.* **17,** 4180–4189
59. Bernales, S., McDonald, K., and Walter, P. (2006) *PLoS Biol.* **4,** 2311–2324
60. Komatsu, M., Waguri, S., Ueno, T., Iwata, J., Murata, S., Tanida, I., Ezaki, J., Mizushima, N., Ohsumi, Y., Uchiyama, Y., Kominami, E., Tanaka, K., and Chiba, T. (2005) *J. Cell Biol.* **169,** 425–434
61. Liljedahl, M., Maeda, Y., Colanz, A., Ayala, I., Lint, J. V., and Malhotra, V. (2001) *Cell* **104,** 409–420
62. Hu, J., Shibata, Y., Voss, C., Shemesh, T., Li, Z., Coughlin, M., Kozlov, M. M., Rapoport, T. A., and Prinz, W. A. (2008) *Science* **5867,** 1247–1250
63. Shibata, Y., Voss, C., Rist, J. M., Hu, J., Rapoport, T. A., Prinz, W. A., and Voeltz, G. K. (2008). *J. Biol. Chem.* **283,** 18890–18904